Formation of plateau landscapes on glaciated continental margins

David L. Egholm[1]*, John D. Jansen[1,2], Christian F. Brædstrup[1], Vivi K. Pedersen[3], Jane L. Andersen[1], Sofie V. Ugelvig[1], Nicolaj K. Larsen[1] and Mads F. Knudsen[1]

Low-relief plateaus separated by deeply incised fjords are hallmarks of glaciated, passive continental margins. Spectacular examples fringe the once ice-covered North Atlantic coasts of Greenland, Norway and Canada, but low-relief plateau landscapes also underlie present-day ice sheets in Antarctica and Greenland. Dissected plateaus have long been viewed as the outcome of selective linear erosion by ice sheets that focus incision in glacial troughs, leaving the intervening landscapes essentially unaffected. According to this hypothesis, the plateaus are remnants of preglacial low-relief topography. However, here we use computational experiments to show that, like fjords, plateaus are emergent properties of long-term ice-sheet erosion. Ice sheets can either increase or decrease subglacial relief depending on the wavelength of the underlying topography, and plateau topography arises dynamically from evolving feedbacks between topography, ice dynamics and erosion over million-year timescales. This new mechanistic explanation for plateau formation opens the possibility of plateaus contributing significantly to accelerated sediment flux at the onset of the late Cenozoic glaciations, before becoming stable later in the Quaternary.

G lobal cooling in the late Cenozoic caused periodic growth of vast ice sheets that blanketed the North Atlantic continental margins. The resultant insertion of 2–3-km-deep fjords epitomizes positive feedbacks between bedrock lowering and ice dynamics that focus incision in fjords[1,2] while limiting the erosive potential on the high, interfjord plateaus[3–12]. However, unlike fjords, which are the unequivocal products of glacial erosion, the enigmatic origin of the interfjord plateaus has fuelled long and vigorous debate[13–16]. A key point of contention is the role of glaciers as amplifiers of relief. Glaciers have created some of Earth's steepest and highest relief; hence, in keeping with selective linear erosion, the low, rolling relief of the high plateaus has been regarded as incompatible with a glacial origin[3–7,13,16]. On the continental margins where they are well developed, such as eastern Canada[4,6], Greenland[3] and Norway[5,13] (Fig. 1), plateau landscapes are therefore assumed to retain the shape of their 'ancient preglacial' roots despite being repeatedly overridden by ice sheets[3–7,13,16].

Several factors are consistent with the preglacial hypothesis. Long-term preservation of the plateau surfaces fits with cosmogenic nuclide abundances indicating that overriding ice in many cases removed less than a few metres of bedrock over the past few glaciations[6,8–12]. Accordingly, many summit plateaus host regolith mantles developed via long-term physical and chemical weathering, with few signs of recent glacial erosion[17–21]. In addition, systematic variations in nuclide abundances with elevation indicate that bedrock erosion rates generally increase with depth into the glacial troughs[6,9–12], consistent with selective linear erosion[22]. These observations are widely explained by the development of non-erosive, frozen-bed patches under successive ice sheets and have been used to assert that the late Cenozoic glaciations left the North Atlantic high plateaus largely undisturbed[3–7,13,16]. However, such reasoning implies that recent ice-sheet behaviour can be extrapolated back across the preceding glaciations, and overlooks two important aspects of the regional

landscape evolution: firstly, isostatic uplift associated with erosional unloading in fjords has gradually increased the elevation of the plateaus; and secondly, as relief evolves more ice is drained from the plateaus into the fjords thereby thinning ice at high elevations and lowering subglacial temperatures[1,2,10]. Other studies therefore question the veracity of the preglacial hypothesis and argue instead that plateau and fjord landscapes have been continuously eroding, although at rates that vary through time[14,15].

Computational experiments

To investigate how overriding ice sheets may have shaped the topography of passive continental margins, we used the iSOSIA ice-sheet model[23] to perform computational landscape-evolution experiments (see Methods). The initial topography was designed to represent a small part of a continental margin prior to glaciation. For this, we used a modelled non-glacial, fluvial-type landscape without plateau topography and a starting total relief of 1,000 m (Fig. 2). The grid was 100 km × 50 km, which is large enough to include several fjords and plateaus, while still allowing ice flow to be modelled using a grid resolution of only 200 m. The two short-side boundaries were reflective, meaning that topography and modelled erosion can be mirrored infinitely in the direction perpendicular to these two grid boundaries. We simulated glaciation by blanketing the landscape with an ice sheet where the upper surface was sloping gently (1.5%) coastward. The ice cover was up to 1,000 m thick, which was just enough to keep all of the landscape buried in ice throughout the experiments. The ice was allowed to creep and slide across the landscape and the rate of subglacial bedrock erosion was assumed to scale with the square of the sliding rate[24–26] (see Methods). The ice surface was allowed to change form in response to the flow, but remained a smoothly undulating low-relief surface during the simulation. The model domain was assumed to be located close to the glacial equilibrium line altitude, with negligible
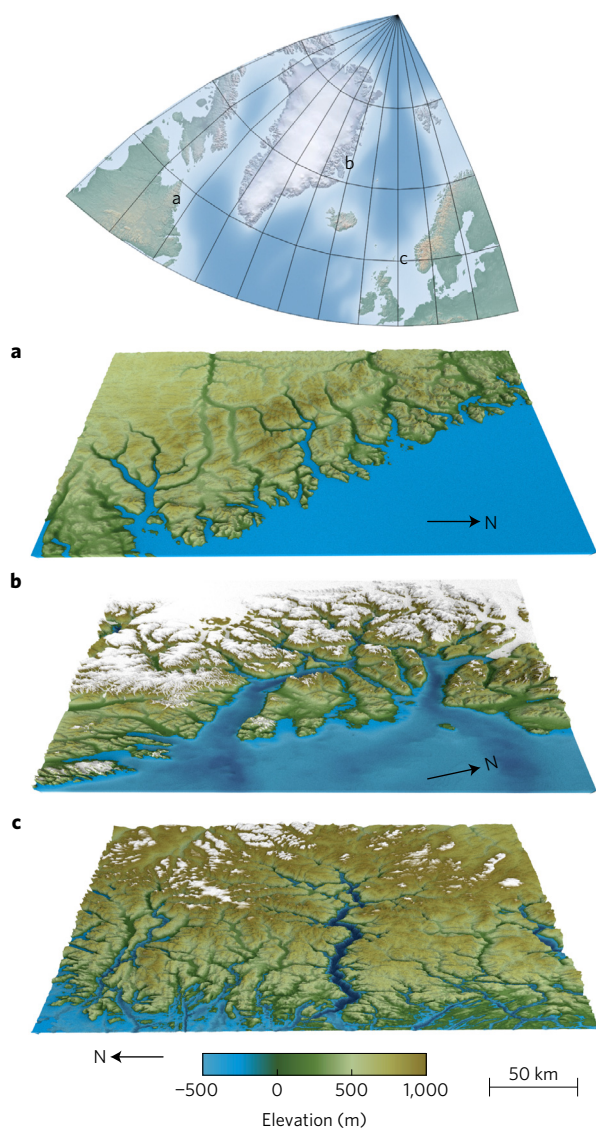
Figure 1 | Examples of high-elevation plateau landscapes in the North Atlantic region. a, The Torngat Mountains in eastern Canada. **b**, East Greenland coast around Kong Oscar Fjord and Kejser Franz Joseph Fjord. **c**, Southern Norway around Sognefjorden.

net surface accumulation/ablation; the total ice flux in and out of the model hence remained constant. The computational experiments spanned 500 kyr of continuous glaciation; a period approximately matching that of cumulative Quaternary ice-sheet glaciation along the now ice-free parts of the Scandinavian Mountains in Norway (using a benthic foraminifera δ^{18}O glaciation threshold of 4.2‰, Fig. 2)[7,27]. Our computational experiments included flexural isostasy in response to erosional unloading of the underlying crust and mantle, but ignored non-glacial erosion mechanisms, such as fluvial and periglacial erosion. Furthermore, while glaciological parameters such as ice thickness, ice flux and mass balance clearly varied through time along real glaciated continental margins, we deliberately simplified our experiments by keeping such parameters constant through time to most effectively target the following questions: how does ice-sheet erosion across different length scales influence the relief of the underlying landscape, and to what degree can first-order feedbacks between ice dynamics, glacial erosion and flexural isostasy explain plateau topography?

To test the robustness of our findings, we conducted additional experiments with varying ice thickness, initial relief, lithosphere

flexural rigidity, glacial erosion model, ice flux and surface temperature. We return to the outcome of this sensitivity analysis below.

Relief planation by ice sheets

A robust first-order outcome of our computational experiments is a positive feedback between erosion and topographic relief in the main valleys: subglacial sliding becomes progressively localized and the total ice flux evolves from nearly uniform to highly channelized (Fig. 2b). The channelized flow accelerates valley deepening and eventually cuts fjords below sea level such that total relief increases from the initial 1 km to >2 km (−1,000 to 1,400 m.a.s.l.). This development and the positive feedback driving it is in close agreement with previous modelling results[1,28]. However, our higher-order ice model delivers new insights regarding the evolution of interfjord uplands (Figs 2 and 3). Here, subglacial erosion reduces local relief because topography generally fluctuates at length scales shorter than those occurring within the ice-flow velocity field.

Thick ice cannot readily adapt its flow to the details of the underlying topography because horizontal stress gradients counteract velocity variations over short distances[29–31]. The total velocity (the sum of subglacial sliding and ice creep) is thus relatively constant across small-scale ridges and valleys, but the accompanying variations in local ice thickness cause differences in the partitioning of motion into sliding versus creep. Subglacial sliding is faster over ridges because thinner ice reduces the contribution of creep to the total velocity and sliding must accelerate to compensate. Faster sliding over ridges increases erosion and therefore reduces short-range topographic relief (Fig. 3).

The resultant flatter surfaces rise in elevation because total erosion (∼50–300 m) is exceeded by flexural isostatic uplift (∼400 m) due to erosional unloading caused by fjord incision (Supplementary Fig. 1). The final overall plateau morphology (Fig. 2b, bottom panel) is the culmination of reduced short-range (<2 km) relief coupled with uplift and low-angle flexural isostatic tilting in the direction opposite to ice flow. The final relief distribution across the modelled plateaus matches that observed, for example, in southern Norway (Supplementary Fig. 2).

Short-range smoothing of topography under ice sheets hence occurs due to fundamental ice dynamics related to horizontal stress gradients that arise because ice is a viscous material. Horizontal stress gradients are not included in standard shallow-ice models[1,28]; their effects can be simulated only via full-Stokes or higher-order ice models such as the one used here. To explore how horizontal stress gradients affect subglacial erosion in a more conceptual manner, we performed a set of even simpler experiments in which an ice sheet flows across sinusoidal topography. We found that where a 1,000-m-thick ice sheet flows parallel to uniformly spaced valleys and ridges in a setting of homogeneous bedrock, relief is likely to decrease for valley spacings <2 km (Supplementary Fig. 3).

Because planation is an inherent result of viscous ice flow across undulating bed topography, it is not sensitive to the detailed choice of model parameterization of, for example, basal sliding or subglacial erosion. Variations in parameters such as erosion-law scaling constants and boundary ice flux work only to increase or decrease the pace at which planation works, while the spatial patterns of erosion remain the same. Ice thickness, mass balance and ice-surface temperature influence the thermal conditions of the ice bed. Hence, thin ice, high rates of ice accumulation, and low surface temperature promote non-erosive cold-based conditions on plateaus more quickly (Supplementary Fig. 4). The resulting level of plateau planation thus depends on these parameters, but the overall tendency is the same: short-range relief decreases as long as warm-based erosive conditions are maintained at the bed. Likewise, the tendency for plateau planation is independent of initial relief (Supplementary Fig. 5), lithosphere flexural rigidity (Supplementary Fig. 1) or choice of erosion law (Supplementary Fig. 6), confirming
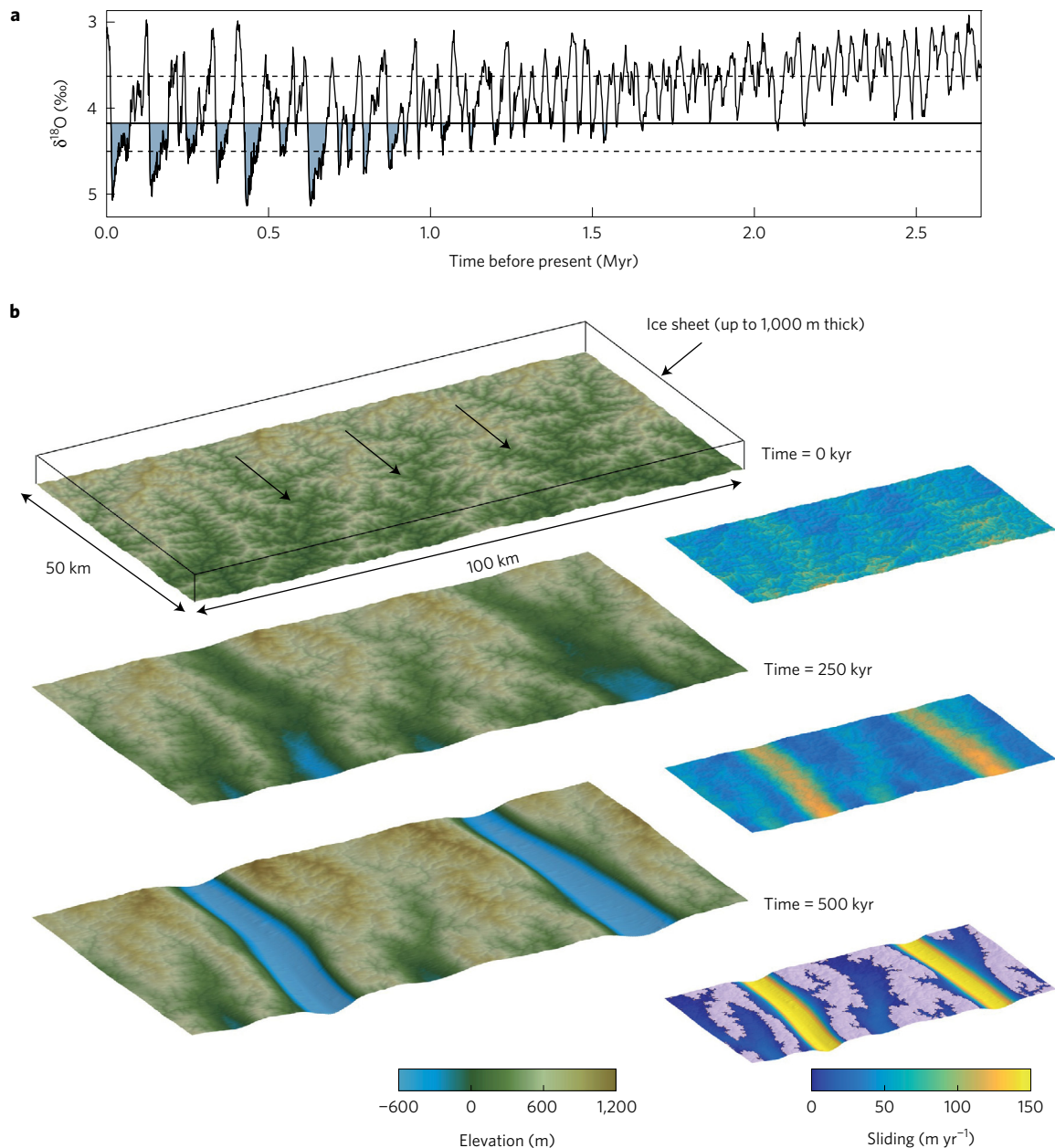
Figure 2 | Modelled evolution of a continental margin landscape undergoing ice-sheet erosion and flexural isostasy. a, The assumed glaciation history illustrated using the benthic foraminifera δ^{18}O record[27]. The glacial periods (in total 500 kyr) are blue. **b**, Left-side panels show the topographic evolution of the subglacial landscape over time (completely ice-covered throughout the simulation). Upper to lower panels: the initial non-glacial landscape, then after 250 and 500 kyr of glaciation, respectively. Initial landscape relief is 1 km (from 0 to 1,000 m.a.s.l.). Right-side panels show the corresponding distribution of sliding velocity; frozen-bed patches with neither sliding nor erosion are shown as light grey areas.

that, although variation in parameters may affect its efficiency, the plateau-forming mechanism is a predictable consequence of deep erosion by ice sheets along continental margins.

While the resolution of our model (200 m) cannot fully resolve the fine-scale morphology of real plateau landscapes, our results suggest that large-scale (>1 km) preglacial drainage patterns are largely preserved, albeit in a subdued form (Figs 2 and 3). Widespread ice-sheet erosion is therefore compatible with survival of landforms as described in previously glaciated 'palaeic' terrain[7,16,32]. We note, however, that by focusing solely on ice-sheet erosion our experiments neglect other erosion processes that may have influenced relief development, particularly between glaciations. For example, small valley glaciers may counteract plateau development by increasing local relief between glacial valleys and

unglaciated ridges[16,22]. This point is relevant for higher massifs, such as Jotunheimen in southern Norway (Supplementary Fig. 2), which intersect the snowline altitude during interglacial periods. In lower areas or those lacking the ridges required to host alpine glaciers, periglacial surface processes, including frost cracking of bedrock and frost creep of soil, probably dominated the interglacials. Such processes are known to reduce local relief and hence further promote plateau development[33–35].

The pace of erosion evolves over time

Several first-order feedbacks contribute to the evolution of patterns and rates of erosion as fjords progressively deepen and plateaus are hoisted to higher elevations by flexural isostasy. Whereas erosion accelerates in fjord troughs, as shown previously by others[1],
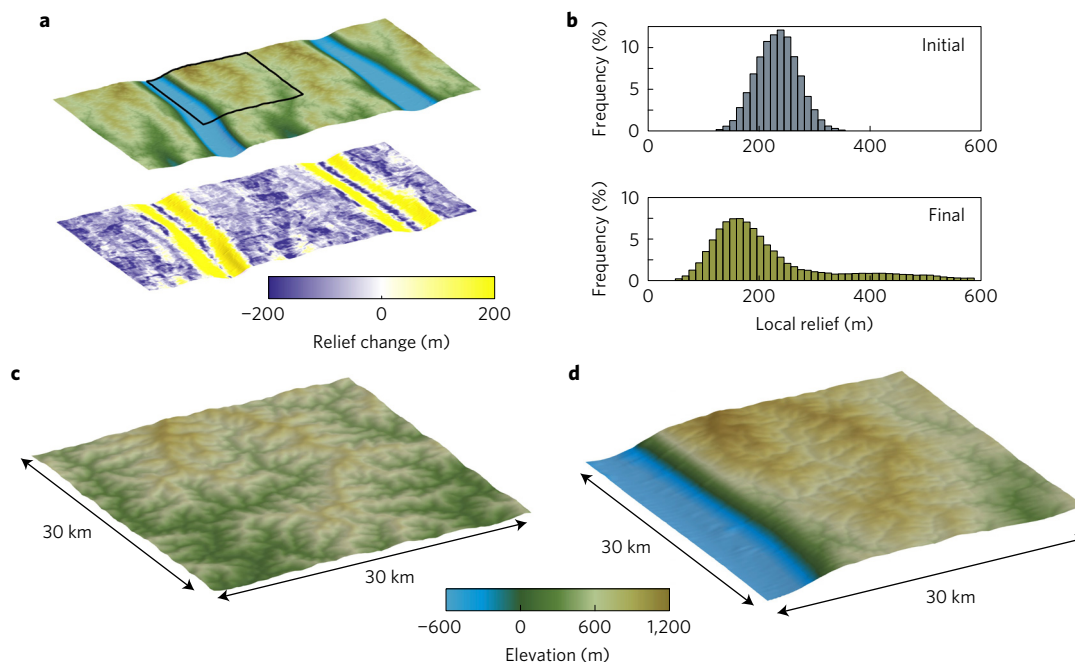
Figure 3 | Evolution of local topographic relief in response to ice-sheet erosion. Local relief was measured in the computational experiments as the difference between maximum and minimum elevation in 2 by 2 km square windows centred in each 200 m grid cell. **a**, Final topography (upper panel) and change in local relief due to glacial erosion (lower panel). **b**, Frequency distribution of local relief before and after glacial erosion. Note that local relief increased in specific areas (adjacent to emerging fjords), but glacial erosion diminished local relief over most areas. **c**,**d**, Detailed topography before and after glacial erosion; black box in **a** indicates the location of **c** and **d**.

erosion rates decrease across the high plateaus for two reasons: as troughs deepen, progressively more ice is funnelled through them rather than over plateaus; and as plateaus are isostatically raised, the overriding ice thins, which in turn drives down basal ice temperature while simultaneously increasing the pressure-melting point. With time, this leads to widespread development of frozen-bed patches (Fig. 2), which impedes subglacial sliding and hence preserves rather than erodes bedrock. In other words, owing to the topographic evolution, the interfjord uplands experience a major switch from warm-based, erosive conditions before fjord incision to cold-based, non-erosive conditions after fjord incision[2]. Accordingly, the spatial distribution of subglacial sliding and erosion rate changes dramatically over time (Fig. 2). Early in our simulations, shortly after the onset of glaciation, erosion rates are nearly uniform across the landscape (100 to 300 mm kyr^{-1}), but this evolves into a highly bimodal array spanning three orders of magnitude from <1 mm kyr^{-1} to >2,000 mm kyr^{-1} (Fig. 4). The stark contrast in final erosion rates results from the dynamic decoupling of fast-flowing ice in fjords from slowly flowing cold-based ice covers on the emergent plateaus. The modelled rates of erosion are in general agreement with rates estimated from glacial sediment yields and cosmogenic nuclide analysis[25,36,37].

Predictions of erosion rates that were orders-of-magnitude faster during early glaciations invite us to speculate that interfjord plateaus were a major source of erosional flux that coincided with intensified cooling in the late Cenozoic[38] (Fig. 4c). In our experiments, roughly one-third of the total sediment yield is sourced from plateaus between 500 and 1,000 m elevation (Fig. 4c). Even modest depths of plateau erosion, such as the 100–400 m estimated for interfjord landscapes in Norway[14], translate to globally significant sediment volumes when projected to other glaciated passive margins.

Empirical constraints from cosmogenic nuclides

An important upshot of the evolving erosion patterns is that recent ice-sheet behaviour, inferred from present-day observations and measurements, cannot be extrapolated reliably back to earlier glaciations. This is especially pertinent to extensive cosmogenic nuclide data indicating very low erosion rates on the high plateaus[6,8–12,39,40]. As the production of cosmogenic nuclides is mainly restricted to the upper few metres of the surface, even apparent exposure ages >100 kyr do not necessarily preclude several hundred metres of plateau erosion during early glaciations[41]. To predict the cosmogenic nuclide concentrations resulting from the modelled erosion history (Figs 2 and 3), we punctuated the modelled 500 kyr erosion history with non-erosive ice-free periods inferred from a glaciation δ^{18}O threshold of 4.2‰ (Fig. 2 and Supplementary Fig. 7). We then integrated the cosmogenic nuclide production and decay in every point of the modelled landscape (see Supplementary Fig. 7 and Methods). The resulting cosmogenic nuclide inventory replicates first-order patterns of ^{10}Be abundances on plateau landscapes in Canada[6,12], Greenland[9] and Norway[39] (Fig. 4d and Supplementary Fig. 7). Predicted apparent exposure ages range from the last deglaciation ∼12 kyr ago to >150 kyr at high elevations (Fig. 4d), while ^{26}Al/^{10}Be ratios vary from the production ratio of 6.75 down to 5.75 (Supplementary Fig. 7). The ratio falls below 6.75 when the landscape is buried for long intervals by thick non-erosive ice; hence, we anticipate even lower ratios in cases where ice sheets formed at an earlier time (that is, pre-Quaternary) than in our experiments. Lengthy glacial burial is particularly relevant for the polar regions of Canada[6,10,12], Greenland[9,37], Svalbard[42] and Antarctica[40].

The final stages of our computational experiments echo the essential relationship observed today between erosion rate and elevation (that is, erosion rates decrease with increasing elevation)[6,11,12], and the preservation of plateau landscapes via frozen-bed patches is shown to be the predictable outcome of long-term topographic feedbacks associated with fjord incision (Fig. 2). Indeed, our results are fully consistent with the hypothesis of selective linear erosion[3,4,6,16], except regarding the origin and evolution of the plateaus. Rather than being remnants from preglacial times, we propose that the plateau landscapes reflect glacial and periglacial smoothing of
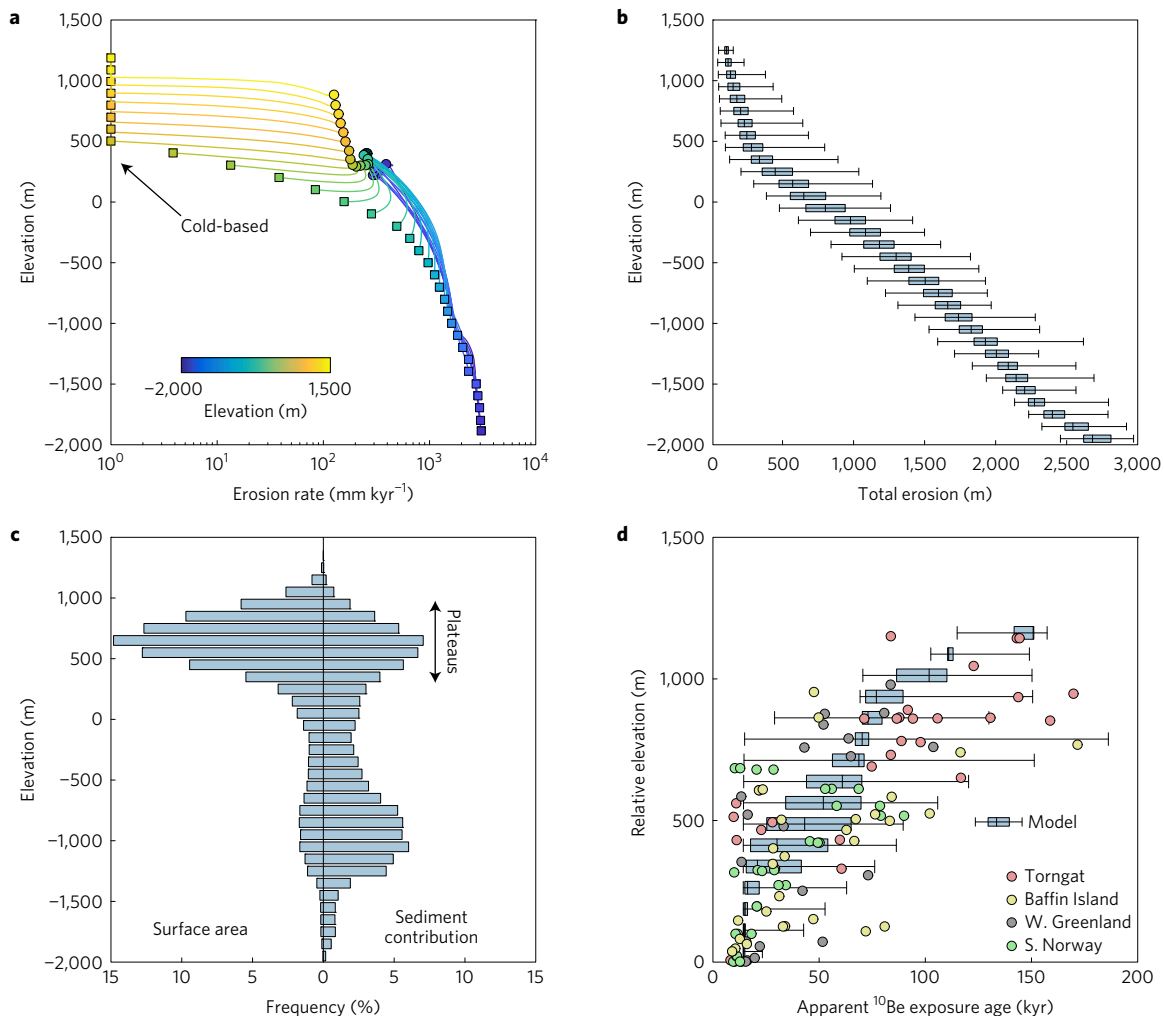
Figure 4 | Erosion history and cosmogenic nuclide apparent exposure ages. a, Average erosion rates binned at 100 m elevation intervals before (circles) and after (squares) glacial erosion (binning follows final elevation). **b**, Distribution of total erosion with elevation. **c**, Distribution of surface area (after glaciation) and sediment yield with elevation. **d**, Modelled apparent [10]Be ages with elevation, compared to published [10]Be ages (coloured dots) predating last deglaciation from the Torngats[6], Baffin Island[12], West Greenland[9] and southern Norway[39]. Note that [10]Be age elevations are relative only (that is, vertical axis shows elevation above lowest data point). Box-and-whiskers in **b** and **d** represent 5th, 25th, 50th, 75th and 95th percentiles within each elevation bin.

terrain that was already high prior to the inception of glaciers and was raised higher by isostatic uplift in response to deep fjord erosion. This does not exclude the possibility that long-term chemical and physical weathering was already actively shaping low-relief regolith-covered landscapes in the old Palaeozoic mountain ranges flanking the North Atlantic[15,16,43], but we propose that widespread erosion by early ice sheets played a major role in forming the current plateau topography.

Methods

Methods, including statements of data availability and any associated accession codes and references, are available in the online version of this paper.

References

1. Kessler, M. A., Anderson, R. S. & Briner, J. P. Fjord insertion into continental margins driven by topographic steering of ice. *Nat. Geosci.* **1,** 365–369 (2008).
2. Refsnider, K. A. & Miller, G. H. Reorganization of ice sheet flow patterns in Arctic Canada and the mid-Pleistocene transition. *Geophys. Res. Lett.* **37,** L13502 (2010).
3. Sugden, D. E. in *Progress in Geomorphology* Vol. 7 (eds Brown, E. H. & Waters, R. S.) 177–195 (Institute of British Geographers Special Publications, 1974).
4. Sugden, D. E. Glacial erosion by the Laurentide ice sheet. *J. Glaciol.* **20,** 367–391 (1978).
5. Nesje, A. & Whillans, I. M. Erosion of Sognefjord, Norway. *Geomorphology* **9,** 33–45 (1994).
6. Staiger, J. K. W. *et al*. Quaternary relief generation by polythermal glacier ice. *Earth Surf. Process. Landforms* **30,** 1145–1159 (2005).
7. Kleman, J. & Stroeven, A. P. Preglacial surface remnants and Quaternary glacial regimes in northwestern Sweden. *Geomorphology* **19,** 35–54 (1997).
8. Fabel, D. *et al*. Landscape preservation under Fennoscandian ice sheets determined from *in situ* produced [10]Be and [26]Al. *Earth Planet. Sci. Lett.* **201,** 397–406 (2002).
9. Corbett, L. B., Bierman, P. R., Graly, J. A., Neumann, T. A. & Rood, D. H. Constraining landscape history and glacial erosivity using paired cosmogenic nuclides in Upernavik, northwest Greenland. *Geol. Soc. Am. Bull.* **125,** 1539–1553 (2013).
10. Briner, J. P. *et al*. Using *in situ* cosmogenic [10]Be, ^{14}C, and [26]Al to decipher the history of polythermal ice sheets on Baffin Island, Arctic Canada. *Quat. Geochronol.* **19,** 4–13 (2014).
11. Li, Y. *et al*. Ice sheet erosion patterns in valley systems in northern Sweden investigated using cosmogenic nuclides. *Earth Surf. Process. Landforms* **30,** 1039–1049 (2005).
12. Briner, J. P., Miller, G. H., Davis, P. T. & Finkel, R. C. Cosmogenic radionuclides from fjord landscapes support differential erosion by overriding ice sheets. *GSA Bull.* **118,** 406–420 (2006).

13. Lidmar-Bergström, K., Ollier, C. D. & Sulebak, J. R. Landforms and uplift history of southern Norway. *Glob. Planet. Change* **24,** 211–231 (2000).
14. Steer, P., Huismans, R. S., Valla, P. G., Gac, D. & Herman, F. Bimodal Plio-Quaternary glacial erosion of fjords and low-relief surfaces in Scandinavia. *Nat. Geosci.* **5,** 635–639 (2012).
15. Nielsen, S. B. *et al*. The evolution of western Scandinavian topography: a review of Neogene uplift versus the ICE (isostasy-climate-erosion) hypothesis. *J. Geodynam.* **47,** 72–95 (2009).
16. Hall, A. M., Ebert, K., Kleman, J., Nesje, A. & Ottesen, D. Selective glacial erosion on the Norwegian passive margin. *Geology* **41,** 1203–1206 (2013).
17. Ballantyne, C. K. Age and significance of mountain-top detritus. *Permafr. Periglac. Process.* **9,** 327–345 (1998).
18. Fjellanger, J. *et al*. Glacial survival of blockfields on the Varanger Peninsula, northern Norway. *Geomorphology* **82,** 255–272 (2006).
19. Marquette, G. C. *et al*. Felsenmeer persistence under non-erosive ice in the Torngat and Kaumajet mountains, Quebec and Labrador, as determined by soil weathering and cosmogenic nuclide exposure dating. *Can. J. Earth Sci.* **41,** 19–38 (2004).
20. Goodfellow, B. W. *et al*. Arctic-alpine blockfields in the northern Swedish Scandes: late Quaternary—not Neogene. *Earth Surf. Dynam.* **2,** 383–401 (2014).
21. Rea, B. R., Whalley, B. W., Rainey, M. M. & Gordon, J. E. Blockfields, old or new? Evidence and implications from some plateaus in northern Norway. *Geomorphology* **15,** 109–121 (1996).
22. Sugden, D. E. & John, B. S. *Glaciers and Landscape: a Geomorphological Approach* (Edward Arnold, 1976).
23. Egholm, D. L., Knudsen, M. F., Clark, C. D. & Lesemann, J. E. Modeling the flow of glaciers in steep terrains: the integrated second-order shallow ice approximation (iSOSIA). *J. Geophys. Res.* **116,** F02012 (2011).
24. Hallet, B. A theoretical model of glacial abrasion. *J. Glaciol.* **23,** 39–50 (1979).
25. Koppes, M. *et al*. Observed latitudinal variations in erosion as a function of glacier dynamics. *Nature* **526,** 100–103 (2015).
26. Herman, F. *et al*. Erosion by an Alpine glacier. *Science* **350,** 193–195 (2015).
27. Lisiecki, L. E. & Raymo, M. E. A Pliocene–Pleistocene stack of 57 globally distributed benthic d18O records. *Paleoceanography* **20,** PA1003 (2005).
28. Jamieson, S. S. R., Hulton, N. R. J. & Hagdorn, M. Modelling landscape evolution under ice sheets. *Geomorphology* **97,** 91–108 (2008).
29. Gudmundsson, G. H. Transmission of basal variability to a glacier surface. *J. Geophys. Res.* **108,** 2253 (2003).
30. Pelletier, J. D., Comeau, D. & Kargel, J. Controls of glacial valley spacing on Earth and Mars. *Geomorphology* **116,** 189–201 (2010).
31. Egholm, D. L., Pedersen, V. K., Knudsen, M. F. & Larsen, N. K. On the importance of higher order ice dynamics for glacial landscape evolution. *Geomorphology* **141–142,** 67–80 (2012).
32. Reusch, H. Nogle Bidrag till Forstaalesen af hvorledes Norges Dale og Fjelde er blevne til. *Norges Geologiske Undersøkelse* **32,** 124–263 (1901).
33. Small, E. E., Anderson, R. S. & Hancock, G. S. Estimates of the rate of regolith production using ¹⁰Be and ²⁶Al from an alpine hillslope. *Geomorphology* **27,** 131–150 (1999).
34. Anderson, R. S. Modeling the tor-dotted crests, bedrock edges, and parabolic profiles of high alpine surfaces of the Wind River Range, Wyoming. *Geomorphology* **46,** 35–58 (2002).
35. Egholm, D. L., Andersen, J. L., Knudsen, M. F., Jansen, J. D. & Nielsen, S. B. The periglacial engine of mountain erosion—Part 2: modelling large-scale landscape evolution. *Earth Surface Dynam.* **3,** 463–482 (2015).
36. Hallet, B., Hunter, L. & Bogen, J. Rates of erosion and sediment evacuation by glaciers: a review of field data and their implications. *Glob. Planet. Change* **12,** 213–235 (1996).
37. Strunk, A. *et al*. One million years of glaciation and denudation history in West Greenland. *Nat. Commun.* **8,** 14199 (2017).
38. Zhang, P., Molnar, P. & Downs, W. R. Increased sedimentation rates and grain sizes 2–4 Myr ago due to the influence of climate change on erosion rates. *Nature* **410,** 891–897 (2001).
39. Linge, H. *et al*. *In situ* ¹⁰Be exposure ages from southeastern Norway: implications for the geometry of the Weichselian Scandinavian ice sheet. *Quat. Sci. Rev.* **25,** 1097–1109 (2006).
40. Sugden, D. E. *et al*. Selective glacial erosion and weathering zones in the coastal mountains of Marie Byrd Land, Antarctica. *Geomorphology* **67,** 317–334 (2005).
41. Young, N. E., Briner, J. P., Maurer, J. & Schaefer, J. M. ¹⁰Be measurements in bedrock constrain erosion beneath the Greenland Ice Sheet margin. *Geophys. Res. Lett.* **43,** 2016GL070258 (2016).
42. Gjermundsen, E. F. *et al*. Minimal erosion of Arctic alpine topography during late Quaternary glaciation. *Nat. Geosci.* **8,** 879–792 (2015).
43. Krabbendam, M. & Bradwell, T. Quaternary evolution of glaciated gneiss terrains: pre-glacial weathering vs. glacial erosion. *Quat. Sci. Rev.* **95,** 20–42 (2014).

Author contributions

D.L.E. designed the study and developed the computational modelling scheme. D.L.E. and C.F.B. performed the computational experiments. D.L.E., J.D.J. and C.F.B. interpreted results. D.L.E., J.D.J., C.F.B. and V.K.P. wrote the paper with contributions from co-authors.

Additional information

Supplementary information is available in the online version of the paper. Reprints and permissions information is available online at www.nature.com/reprints. Publisher's note: Springer Nature remains neutral with regard to jurisdictional claims in published maps and institutional affiliations. Correspondence and requests for materials should be addressed to D.L.E.

Competing financial interests

The authors declare no competing financial interests.

Methods

Experimental design. The computational landscape-evolution model was designed to study patterns of subglacial erosion when a small portion of an ice sheet creeps and slides across a fully submerged bedrock landscape. Interglacial periods and intervals with variable ice cover were not included in the simulation. Likewise, while we acknowledge the influence of rock type and bedrock fracture density on subglacial erosion[44,45] as shown for example by lithologically controlled steps at the Norway and Greenland margins[46,47], we did not include such complexities here because we aimed to most effectively focus on large-scale feedbacks between topography, ice flow, glacial erosion and flexural isostatic adjustments.

The experimental set-up used initial topography generated by a fluvial landscape-evolution model. The fluvial topography could for example represent a slowly decaying remnant of the Caledonian mountains flanking parts of the North Atlantic, or it could be the remains of a rift flank formed prior to breakup of the Atlantic. To form such fluvial topography, an initially flat landscape (a 50×100 km rectangular grid) at sea level was uplifted at a constant rate, while keeping grid cells at sea level along one grid boundary. Channels were allowed to incise the rising landscape with rates scaled by the stream-power equation[48] until a steady-state balance between uplift and erosion was met at every point of the grid. Total relief was at this stage 1,000 m, from sea level to maximum elevation (Fig. 2).

The fluvial-type landscape was then transferred to the glacial landscape-evolution model and used as the starting point for our computational experiments. The initial landscape was covered by an ice sheet with a gently sloping surface ranging from 1,000 m to 2,000 m in elevation, parallel to the regional bed slope (Fig. 2). In the model, total ice flux was kept constant through both grid boundaries perpendicular to ice flow. The boundary flux was fixed at 7×10^9 m³ yr⁻¹, which resulted in realistic levels of both sliding and creep velocities (Fig. 2). A zero-flux free-slip condition was imposed on grid boundaries parallel to ice flow (the short 50 km boundaries). The elevation of the ice surface away from the grid boundaries was allowed to freely adjust as ice flow reorganized in response to the changing bed topography. The entire model grid remained fully ice-covered during the model simulation.

Ice-sheet modelling. Ice flow was simulated using the iSOSIA ice model[23]. iSOSIA is a higher-order ice model that includes horizontal stress gradients, which are especially important for this study as they provide local coupling of ice flow and impede short-range gradients in ice velocity. iSOSIA is a two-dimensional, depth-integrated model. The depth integration increases the computational efficiency to allow simulations over 10^5–10^6 yr timescales. The depth-averaged ice-creep velocities were computed from Glen's flow law for ice:

$$\varepsilon_{ij} = A\tau_e^{n-1}s_{ij}$$

where ε_{ij} and s_{ij} are the deviatoric components of the strain rate and stress tensors respectively; τ_e is effective stress; and n and A are ice-creep parameters (Supplementary Table 1). The rate of subglacial sliding, u_b, was computed from the following empirical sliding law[49]:

$$u_b = \frac{B_s}{N}\tau_b^m$$

where τ_b and N are shear stress and effective pressure at the ice bed, respectively; and B_s and m are sliding parameters.

We used a hydrological model in which the subglacial drainage system is described by conduits that can represent both channels and cavities[50]. Owing to the long timescale of the simulations, we ignored diurnal and seasonal pressure variations and used a steady-state version[50] of the hydrological model to estimate long-term average effective hydraulic pressure:

$$N = \left(\frac{k_1 Q\psi + u_b h}{k_2 k_3^{-1/\alpha} Q^{1/\alpha}\psi^{-1/(2\alpha)}}\right)^{1/n}$$

Here Q is water flux; ψ is the hydraulic pressure gradient; u_b is subglacial sliding rate, while k_1, k_2, k_3, α and h are constants (Supplementary Table 1). Because water and ice both flow through the grid, across the up-flow and down-flow grid boundaries, we simply assumed that water flux Q was everywhere 10% of the local ice flux. This assumption does not, however, affect the outcome of the experiments. The hydrological head in the ice remained above sea level during the experiments. The ice was allowed to slide only where the basal ice temperature was at the pressure-melting point. Where ice was colder, sliding and erosion were prohibited. The temperature of the ice was computed using the three-dimensional transient heat equation:

$$\rho c \frac{\partial T}{\partial t} = k\nabla^2 T - \rho c\mathbf{u}\cdot\nabla T + A$$

where T is temperature; $\mathbf{u}$ is the three-component vector of ice velocity; A is heat produced by friction; ρ is ice density; c is specific heat; and k is heat conductivity

(Supplementary Table 1). The heat equation was solved over every time step using a semi-implicit thermal model[51]. This model involves one-dimensional vertical grid profiles through the ice in every grid cell of the two-dimensional iSOSIA grid. When combined, the vertical profiles form a three-dimensional grid structure in which vertical heat transport is updated using an implicit finite-element solver. Heat exchange due to horizontal conduction and advection is handled by explicit time integration[51]. As boundary conditions for the thermal model we used a constant heat flow, q_b, from Earth's crust into the ice, a fixed ice-accumulation rate, M_a, and ice-surface temperature computed from sea-level temperature, T_{sl}, and atmospheric lapse rate, dT_h (Supplementary Table 1). The sea-level temperature and the lapse rate did not change through time.

Glacial erosion. The rate of glacial erosion was assumed to scale with the ice-sliding rate squared:

$$\dot{e}_g = K_e u_b^2$$

The basis for this erosion model is rooted in theoretical models for subglacial abrasion[24] and is also supported by empirical studies[25,26]. We tested the robustness of our findings by exploring two other erosion laws[52] (Supplementary Fig. 5).

Flexural isostasy. The computational experiments included flexural isostasy in response to erosional unloading of the underlying crust and mantle. We used a two-dimensional uniform thin elastic plate model to account for the horizontal strength of the lithosphere:

$$\frac{\partial^4 W}{\partial x^4} + 2\frac{\partial^4 W}{\partial x^2 \partial y^2} + \frac{\partial^4 W}{\partial y^4} = \frac{L}{D}$$

where W is isostatic deflection of the plate; $L = \rho_r gE - \rho_a gW$ is the vertical load on the plate (positive upwards); E is cumulative bedrock erosion in every grid cell; ρ_r and ρ_a are densities of the eroded bedrock and the isostatically compensating asthenosphere, respectively; g is acceleration of gravity; $D = YT_e^3/[12(1-\nu^2)]$ is flexural rigidity where Y is Young's modulus, and ν is Poisson's ratio; and T_e is elastic lithosphere thickness (Supplementary Table 1).

Cosmogenic nuclides. From the erosion histories of the computational experiment presented in Figs 2–4 we computed the abundances of cosmogenic ^{10}Be and ^{26}Al within the surface rocks. The 500 kyr history of glacial erosion (using a δ^{18}O glaciation threshold of 4.2) (refs 7,27) was punctuated by periods of interglacial exposure extending the full model period to 2.6 million years (Supplementary Fig. 7). We assumed zero production of cosmogenic nuclides during glaciations and zero erosion during interglacials.

Nuclide abundances were hence integrated through time according to:

$$N(t+\Delta t) = N(t)e^{-\lambda\Delta t} + \frac{P(z(t))}{\lambda}\left(1 - e^{-\lambda\Delta t}\right)$$

where λ is the nuclide decay constant and Δt is the time-step length. $P(z(t))$ is the production rate at depth z below the bedrock surface. We used a Lagrangian approach in which the burial depth of rocks at the surface is traced back in time[53]. We included production by neutron spallation (P_{sp}), fast muons ($P_{\mu f}$), and slow/negative muons ($P_{\mu n}$):

$$P(z(t)) = P_{sp}(z(t)) + P_{\mu f}(z(t)) + P_{\mu n}(z(t))$$

$$= P_{sp}^0 e^{-\rho_r z(t)/\Lambda_{sp}} + P_{\mu f}^0 e^{-\rho_r z(t)/\Lambda_{\mu f}} + P_{\mu n}^0 e^{-\rho_r z(t)/\Lambda_{\mu n}}$$

where P^0 is the production rate at the surface ($z=0$), ρ_r is bedrock density, and Λ is the attenuation length.

The elevation of grid cells changed trough time in response to erosion and isostatic uplift. The surface production constants (P_{sp}^0, $P_{\mu f}^0$ and $P_{\mu n}^0$) were thus corrected for altitude by:

$$P^0(h) = P^{sl}e^{\rho_{air}h/\Lambda}$$

where P^{sl} is the production constants at sea level, h is elevation above sea level, and ρ_{air} is air density (Supplementary Table 1). Production parameters are from refs 54–56 and are also listed in Supplementary Table 1.

Code availability. All computer codes used are available on request to the corresponding author.

Data availability. The authors declare that data, in the form of computational results, supporting the findings of this study are available within the paper and its Supplementary Information.

References

44. Dühnforth, M., Anderson, R. S., Ward, D. & Stock, G. M. Bedrock fracture control of glacial erosion processes and rates. *Geology* **38,** 423–426 (2010).

45. Krabbendam, M. & Glasser, N. F. Glacial erosion and bedrock properties in NW Scotland: abrasion and plucking, hardness and joint spacing. *Geomorphology* **130,** 374–383 (2011).

46. Fjellanger, J. & Etzelmüller, B. Stepped palaeosurfaces in southern Norway—interpretation of DEM-derived topographic profiles. *Nor. J. Geogr.* **57,** 102–110 (2003).

47. Swift, D. A. *et al*. A reassessment of the role of ice sheet glaciation in the long-term evolution of the East Greenland fjord region. *Geomorphology* **97,** 109–125 (2008).

48. Whipple, K. X. Bedrock rivers and the geomorphology of active orogens. *Annu. Rev. Earth Planet. Sci.* **32,** 151–185 (2004).

49. Budd, W. F., Keage, P. L. & Blundy, N. A. Empirical studies of ice sliding. *J. Glaciol.* **23,** 157–170 (1979).

50. Schoof, C. Ice-sheet acceleration driven by melt supply variability. *Nature* **468,** 803–806 (2010).

51. Egholm, D. L., Pedersen, V. K., Knudsen, M. F. & Larsen, N. K. Coupling the flow of ice, water, and sediment in a glacial landscape evolution model. *Geomorphology* **141–142,** 47–66 (2012).

52. Ugelvig, S. V., Egholm, D. L. & Iverson, N. R. Glacial landscape evolution by subglacial quarrying: a multiscale computational approach. *J. Geophys. Res.* **121,** 2042–2068 (2016).

53. Knudsen, M. F. *et al*. A multi-nuclide approach to constrain landscape evolution and past erosion rates in previously glaciated terrains. *Quat. Geochronol.* **30,** 100–113 (2015).

54. Balco, G., Stone, J. O., Lifton, N. A. & Dunai, T. J. A complete and easily accessible means of calculating surface exposure ages or erosion rates from ^{10}Be and ^{26}Al measurements. *Quat. Geochronol.* **3,** 174–195 (2008).

55. Heisinger, B. *et al*. Production of selected cosmogenic radionuclides by muons: 2. Capture of negative muons. *Earth Planet. Sci. Lett.* **200,** 357–369 (2002).

56. Lifton, N., Sato, T. & Dunai, T. J. Scaling *in situ* cosmogenic nuclide production rates using analytical approximations to atmospheric cosmic-ray fluxes. *Earth Planet. Sci. Lett.* **386,** 149–160 (2014).